






Article

Reptile Search Algorithm (RSA)-Based Selective Harmonic Elimination Technique in Packed E-Cell (PEC-9) Inverter

Rashid Ahmed Khan ¹, Bushra Sabir ¹, Adil Sarwar ², Hwa-Dong Liu ^{3,*} and Chang-Hua Lin ¹

¹ Department of Electrical Engineering, National Taiwan University of Science and Technology, Taipei 106, Taiwan

² Department of Electrical Engineering, ZHCET, Aligarh Muslim University, Aligarh 202002, India

³ Undergraduate Program of Vehicle and Energy Engineering, National Taiwan Normal University, Taipei 106, Taiwan

* Correspondence: hdlu@ntnu.edu.tw; Tel.: +886-2-7749-5953

Abstract: The multilevel inverters (MLIs) are capable of handling large quantities of power and generating high-quality output voltages. Consequently, the size of the filters is reduced, and the circuitry is simplified. As a result, they have a diverse range of uses in the industrial sector, especially in smart grids. The input voltage boosting feature is required to utilize the MLI with renewable energy. In addition, a large number of components are required to attain higher output voltage levels, which increases the cost of the circuit and weight. A variety of MLI topologies have been identified to reduce losses, device quantity, and device ratings. The selective harmonic elimination (SHE) approaches reduce distinct lower order harmonics by computing the ideal switching angles. This research presents a nine-level Packed E-Cell (PEC-9) inverter that uses selective harmonic elimination to eliminate total harmonic distortion. In order to calculate the best switching angle, the reptile search algorithm (RSA) is implemented in this paper, a nature-inspired metaheuristic algorithm inspired by the hunting behavior of the crocodile. The hunting behavior of crocodiles is implemented in two main steps: the first is encircling, which is accomplished by belly walking or high walking, and the second is hunting, which is accomplished by hunting cooperation or hunting coordination. In this technique, nonlinear transcendental equations have been solved. The simulation was run in the MATLAB R2021b software environment. The simulation results suggest that the RSA outperforms the other metaheuristic algorithms. Furthermore, the simulation result was validated on a hardware setup using DSP-TMS320F28379D in the laboratory.

Keywords: multilevel inverter; nine-level Packed E-Cell (PEC-9); reptile search algorithm; selective harmonic elimination



Citation: Khan, R.A.; Sabir, B.; Sarwar, A.; Liu, H.-D.; Lin, C.-H. Reptile Search Algorithm (RSA)-Based Selective Harmonic Elimination Technique in Packed E-Cell (PEC-9) Inverter. *Processes* **2022**, *10*, 1615. <https://doi.org/10.3390/pr10081615>

Academic Editor: Jiaqiang E

Received: 26 July 2022

Accepted: 13 August 2022

Published: 16 August 2022

Publisher's Note: MDPI stays neutral with regard to jurisdictional claims in published maps and institutional affiliations.



Copyright: © 2022 by the authors. Licensee MDPI, Basel, Switzerland. This article is an open access article distributed under the terms and conditions of the Creative Commons Attribution (CC BY) license (<https://creativecommons.org/licenses/by/4.0/>).

1. Introduction

Single direct current (DC) source inverters, such as modular multilevel converters (MMCs) and compact multilevel topologies, are gaining popularity in industrial applications due to their ability to operate at more excellent power ratios [1–4]. The multilevel cascaded H-bridge (CHB) is one of the most intriguing topologies because it may be implemented as a single-DC source compact inverter with additional DC sources replaced by DC capacitors [5–7]. Aside from a large number of components in a single-DC source CHB, the capacitor voltage balance is the most significant difficulty. In multilevel inverters, some control methods for capacitor voltage balancing have been described as high switching frequency methods, which may result in increased power losses. Following the development of the compressed multilevel inverter and the inspiration of the single-DC source CHB inverter, the five-level Packed U-Cell (PUC) inverter [8–10] was introduced, which has a better design than the single-DC source CHB inverter by lowering component counts. The capacitor self-voltage regulation is a significant feature of a five-level PUC inverter;

however, it is a major flaw in voltage balancing when the inverter is enlarged to generate additional step-voltage. Packed E-Cell (PEC), a new single-DC source, single-phase compact multilevel inverter topology that is more optimal than PUC, has recently been introduced [11,12]. The nine-level Packed E-Cell (PEC-9) is a single-phase, single-DC source with seven switches, one auxiliary DC-bus, and two extended horizontal DC capacitors. PEC-9 is constructed optimally by connecting a half bridge to a single-DC source and an E-Cell to a single-DC bus. The E-Cell features five power switches and two DC capacitors, allowing it to provide multiple switching mode conditions to cover the PUC inverter's operation. In addition, as both DC capacitors are simultaneously charged and discharged as they are extended horizontally, the corresponding switching states can be used to successfully regulate the capacitor to the correct reference voltage. Moreover, a low switching frequency solution is aimed at reducing energy loss while also handling the capacitor voltage balance problem [13,14].

Various strategies have been proposed for enhancing inverter performance and output quality [15–17]. The first is to employ various switching algorithms, which include an optimized harmonic-stepped waveform (OHSW), sinusoidal or “subharmonic” natural pulse width modulation (SPWM), optimal total harmonic distortion (THD) minimization (OMTHD), space-vector modulation (SVM), and selective harmonic elimination (SHE) PWM (SHE-PWM). To reduce high-order harmonics, the second option is to use a low pass filter at the output of the inverter. Finally, the third option is adopting multilevel structures to minimize harmonics and THD. Multilevel inverters have also employed the SHE-PWM method [18,19]. It is sought to attain the best harmonics optimization possible if this goal cannot be achieved. The fundamental component can be satisfied, and the (S–1) low-order harmonics from the fifth order can be removed by solving S equations.

This study uses the reptile search algorithm (RSA) to solve the SHE equations in the nine-level Packed E-Cell (PEC-9). This algorithm is more effective and dynamic. It is a newly nature-based metaheuristic optimization algorithm. Crocodiles hunt and encircle each other in real life. The proposed RSA differs from others in that it uses a unique technique to update the low-frequency modulation system, including selective harmonic removal and nearest level control of the solutions utilizing four distinct processes. Encircling, for example, is accomplished by belly walking and high walking. Hunting cooperation or hunting coordination is used to conduct the hunting. The RSA's primary objective is to develop powerful search algorithms that can generate better solutions to challenging problems and generate new best possible results that can aid in resolving complex real-world situations [20]. These attributes were used in the optimization problem-solving algorithm.

The paper has been categorized into six sections. The introduction has been discussed in Section 1. Section 2 provides a quick overview of the metaheuristic algorithm. The working of the RSA has been presented in Section 3. An inverter with a Packed E-Cell 9 (PEC-9) configuration is explained in Section 4. The Implementation of RSA in selective harmonic elimination is explained in Section 5. In Section 6, the simulation findings are discussed. The hardware results are detailed in Section 7, and the conclusion is presented in the final section of the study.

2. Metaheuristic Algorithm

SHE methods are used to eliminate different lower-order harmonics by determining the optimal switching angle. Using the optimization technique, the switching angle can be estimated by solving the nonlinear transcendental equation. Metaheuristic algorithms influence the fields of optimization techniques because of their effectiveness and applications. Metaheuristic algorithms are of two types: population-based and individual-based. In the earlier type, a particular solution is produced, which is improved until the final condition is fulfilled. Although, in the latter type, a set of arbitrary solutions is created until the final situation is satisfied, it continuously improved with numerous operators. Each of these groups has its own individual set of merits and demerits. As a result of the use of

many solutions, population-based meta-heuristics conduct an exploratory analysis. Each iteration explores a different area of the search space. The availability of other solutions in the preferred region is usually assured if a local solution can be captured. Furthermore, the algorithm is less sensitive to population size, even though the constant distribution across all variables improves exploration by the algorithm [18]. Population-based algorithms have the disadvantage of evaluating each solution in the population. As a result, numerous calls to the objective function are necessary, increasing the running time of the algorithm. Population-based algorithms also have a slow convergence rate, which is another disadvantage. Alternatively, individual-based algorithms require only a small amount of space to store each solution during every iteration, and the number of functions evaluated is relatively low. Additionally, it has a fast convergence speed. Despite these benefits, population-based algorithms are prone to local optima stagnation because they use fewer solutions and have less exploratory behavior. For this reason, population-based algorithms are preferred over individual-based algorithms in most fields.

As shown in Figure 1, a population-based algorithm can be divided into a certain type according to the source of inspiration. The evolutionary phenomenon in nature is the main source of inspiration for evolutionary algorithms. The main evolutionary operators in evolutionary algorithms are selection, recombination, and mutation. During optimization, such an algorithm maintains an even rate of exploitation and exploration [21]. Genetic algorithm (GA), differential evolutionary (DE), biogeographical-based optimization (BBO), and swarm-based algorithms, which are spurred by the cumulative activity of a breed of animals that develops global intelligence without a centralized control unit, are among the most well-known evolutionary algorithms. Bee colony optimization (BCO), grey wolf optimizer (GWO), dragonfly algorithm (DFA), particle swarm optimization (PSO), ant colony optimization (ACO), firefly algorithm (FFA), and moth-frame algorithm (MFA) are some of the most popular swarm optimization algorithms [22,23]. Typically, swarm-based algorithms use adaptive mechanisms for fine-tuning exploration and exploitation. Events, behaviors, or phenomena can be used as inspiration for the event-based class. Imperialist competition algorithm (ICA), teaching learning-based optimization (TLBO), and human group formation (HGF) are based on a physical-based algorithm. The physical-based algorithm is inspired by physical phenomena, including the movement and interactions of particles as well as forces between solutions. Gravitational search algorithm (GSA), ray optimization (RO), Archimedes optimization algorithm (AOA), multi-verse optimizer (MVO), and charged system search (CSS) are some of the algorithms based on the class. Algorithms based on mathematics are inspired by various mathematical models and equations. The development of optimization algorithms makes use of a mathematical function model. Radial movement optimization (RMO), sine cosine algorithm (SCA), and hyperspherical search (HSS) algorithm are some of the examples of this class [24].

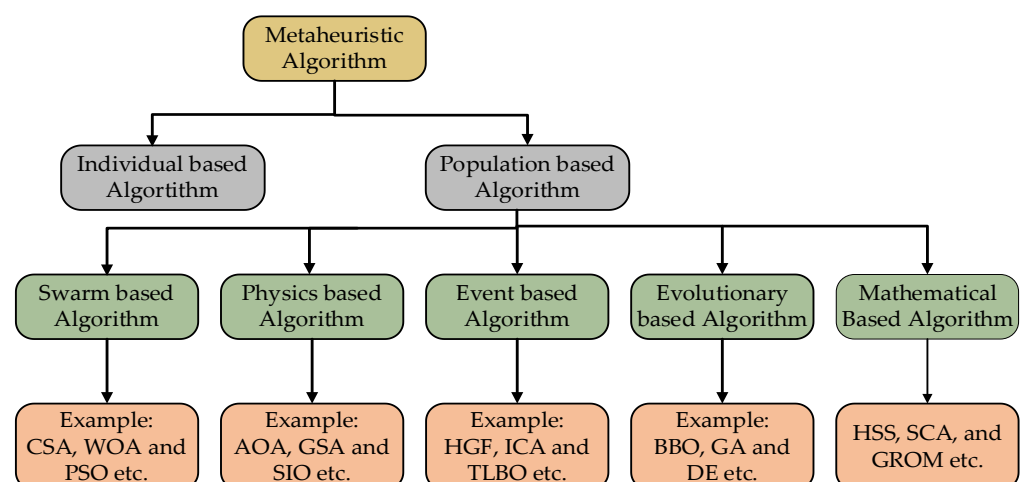


Figure 1. Classification of metaheuristic algorithms.

3. Reptile Search Algorithm

In this section, local search (exploitation) and global search (exploration) stages of the reptile search algorithm (RSA) are addressed, which is obtained by social behavior, encircle techniques, and hug techniques of the nature of crocodiles. The behavior of crocodiles comprises encircling and hunting the victim. To create the proposed RSA and execute the optimization processes, these techniques are mathematically represented. Because RSA is a gradient-free and population-based method, it can be utilized to resolve both complex and simple optimization problems with specified constraints. Cohesive groupings aid active cooperation among crocodiles while also increasing their robustness.

3.1. Crocodile Biology and Behavior

Crocodiles (including real crocodiles) are massive semi-aquatic creepers found across the tropics, including Asia, Australia, Africa, and America. Only the species belonging to the “Crocodylinae” subfamily are referred to as crocodiles. The physical qualities of a crocodile, in general, complement its ability to be a powerful predator. Their exterior shape indicates that they live in water and hunt prey. Crocodiles have a streamlined physique that provides less resistance to air and water flow, allowing them to move quickly. Crocodiles also walk faster by raising their feet to the side. In the water, crocodiles’ webbed feet allow them to quickly navigate around twists and make unexpected movements. These feet are a distinguishing trait, as animals usually walk from one location to another. The following are the main attributes of crocodile behavior.

Vision: Crocodiles have excellent night vision and hunt primarily at night. They take advantage of prey species’ weaknesses (e.g., poor night vision).

Dieting and Hunting: The crocodile is an apex predator, hunting for fish or land animals nearby, then charging at them. Crocodiles eat smaller crocodiles, as well as fish, reptiles, crabs, amphibians, mollusks, birds, and mammals. Crocodiles eat tiny fish and crustaceans first, then move on to bigger prey. Crocodiles are predators (cold-blooded creatures); their slow metabolism allows them to go without food for extended periods of time. Crocodiles, despite their look or lethargic movement, can deliver a powerful punch. They are top predators in their surroundings, and multiple categories were identified. They attack and kill other animals, such as deer and sharks. They would also hunt newborn or dead elephants and other animals if given the opportunity. Evidence shows that crocodiles eat a variety of fruits.

Locomotion: Crocodiles can run extremely quickly over short distances, even when they are not in the water. When a crocodile picks up speed, its legs are kept straight and more straightforward underneath its body (known as high walk). Crocodiles can move at a quick speed when they walk in this way.

Cognition: Crocodiles have sophisticated cognitive abilities. They can identify and use prey behavior patterns, such as when prey comes close to the river to drink regularly.

Hunting: The crocodile hunts cooperatively through collaboration and coordination. Coordination of hunting involves certain predators adjusting their motions to take their prey in a coordinated way while coordinated hunting is being performed. Coordinated hunting is an advanced form of cooperative hunting wherein the specialized predators coordinate with each other’s activities, which is uncommon for a vertebrate-free species. Similar to lions, crocodiles can sometimes play the same function (driver or ambusher) throughout different hunts.

Collaboration and coordination of crocodiles: Crocodiles hunt in groups, according to recent research. This designated them as one of the most intellectual and sophisticated animals, capable of coordinating the efforts of various individuals playing various roles. Observing crocodiles in the act of hunting is a difficult task. Ambush is their preferred method of hunting, and they rarely eat since their metabolisms are slow; almost all of their hunting takes place at night and in shallow water. By grouping, crocodiles forced a dense group of fish to congregate in the same space. A bait ball was thrown after that, so they took turns going after fish from this group. The crocodiles will next take turns attacking the

fishes by cutting across the circular centroid. Crocodiles of varying sizes frequently play a variety of roles. Larger crocodiles lead fish into the shallows of a lagoon, while small, more intelligent crocodiles prohibit them from escaping. A crocodile once startled a zebra or pig (wild beast), causing it to flee into a lagoon where more crocodiles were hiding and ready for the assault. Crocodile hunting behavior is relatively consistent; after catching prey, a crocodile would migrate out of the scouring region and rejoin the other crocodiles. After hunting, it appears that the animals relax and take their turn to rejoin the aggressive hunting group.

The conclusion is that crocodiles are among the most intelligent and skilled hunters, possibly second only to humans. Crocodile behavior was modeled as a mathematical optimization problem, where the goal is to find the optimum solution given a set of restrictions. Numerous quantitative subjects, ranging from engineering, computer science, and economics to operations research and industry, contain optimization problems, and advancements in searching approaches have gained interest in a number of disciplines. The algorithm developed (RSA) was inspired by the process of encircling and chasing prey.

3.2. Initialization Phase

As demonstrated in Equation (1), the optimization process in RSA begins with a collection of candidate solutions (X). It is generated probabilistically, with the best-obtained solution in each iteration regarded to be close to the optimum.

$$X = \begin{bmatrix} x_{1,1} & \dots & x_{1,j} & x_{1,n-1} & x_{1,n} \\ x_{2,1} & \dots & x_{2,j} & \dots & x_{2,n} \\ \dots & \dots & x_{i,j} & \dots & \dots \\ \vdots & \vdots & \vdots & \vdots & \vdots \\ x_{N-1,1} & \dots & x_{N-1,j} & \dots & x_{N-1,n} \\ x_{N,1} & \dots & x_{N,j} & x_{N,n-1} & x_{N,n} \end{bmatrix} \quad (1)$$

By using Equation (2) set of candidate's solutions, X is randomly generated, where j th positions of i th are denoted by $x_{i,j}$, a number of candidate solutions are represented by N , and the given problem dimension size is denoted by n .

$$x_{i,j} = \text{ran} \times (\text{UB} - \text{LB}) + \text{LB}, \quad j = 1, 2, 3, \dots \dots n \quad (2)$$

Here, ran is the random value, and the upper bound and lower bound of the stated problem is denoted by LB and UB , respectively.

3.3. Exploration (Encircling Phase)

The exploratory activity (encircling) of RSA is presented in this section. Crocodiles engage in two movements when encircling: high walk and belly walking, as per their encircling behavior. These movements pertain to various reigns, each of which is dedicated to the exploratory search (globally). Unlike another search phase, crocodile motions (belly and high and walking) do not allow them to reach the objective prey due to their disruption (hunting phase). As a result, the exploration search uncovers a large search region; it may be able to locate the density area after numerous attempts. In addition, during this phase of optimization, the exploration approaches (belly and high walking) are employed to facilitate the other phases of the search process (exploration/hunting) by means of extensive and dispersed study.

This system can alternate between phases of encirclement (exploration) and hunting (exploitation) of the search. Changing between these two behaviors is based on four conditions. All iterations are divided into four sections. Based on two major search approaches, the RSA exploration mechanisms investigate the search regions and approaches to locate the best result (belly walk and high walk strategy).

Two conditions must be met throughout this phase of the search. $t \leq T/4$ is the condition for the movement strategy for a high walk, and $t \leq 2T/4$ and $t > T/4$ is the condition for the movement strategy for a belly walk. This means that for almost half of the exploration iterations (high walk), and another half for belly walk, this requirement will be met. These are two different types of exploration search strategies. A probabilistic scaling coefficient is studied for the element in order to generate a more diverse solution and examine diverse regions. We used the simplest basic guideline, which can be used to simulate the encircling movement of crocodiles. The position update equations for the exploration phase are provided in this study as Equation (3).

$$x_{i,j}(t+1) = \begin{cases} best_j(t) \times -\eta_{(i,j)}(t) \times \beta - R_{i,j}(t) \times ran, & t \leq T/4 \\ best_j(t) \times x_{r1,j} \times ES(t) \times ran, & t \leq 2\frac{T}{4} \text{ and } t > T/4 \end{cases} \quad (3)$$

Here, $best_j(t)$ denotes the j th position in the best solution obtained so far. A random integer between 0 and 1 is denoted by the term ran , T is the maximum number of iterations that can be performed. The current iteration's number is t . The hunting function for the j th position in the i th solution is denoted by the letter $\eta_{(i,j)}$, which is obtained using Equation (4). The sensitive parameter is denoted by β , which influences the surrounding phase exploration precision (high walk) throughout the course of iterations and is set to 0.1. Reduce function indicated by $R_{(i,j)}$, which is a value that is calculated using Equation (5) to reduce the search area. Between $[1 N]$ and $x_{r1,j}$, r_1 is a random number. It denotes the i th solution's random position. The total number of possible solutions is N . A probability ratio called evolutionary sense ($ES(t)$) is derived from Equation (6) by randomly reducing a pair of integers between 2 and -2 across an infinite number of iterations.

$$\eta_{(i,j)} = best_j(t) \times xP_{(i,j)} \quad (4)$$

$$R_{(i,j)} = \frac{best_j(t) - x_{r(2,j)}}{best_j(t) + \epsilon} \quad (5)$$

$$ES(t) = 2 \times r_3 \times \left(1 - \frac{1}{T}\right) \quad (6)$$

Between $[1 N]$, a random number is represented by r_2 , ϵ is a very small value, and 2 is utilized as a correlation value in Equation (6) to provide values between 2 and 0. A random integer value among -1 and 1 is denoted by r_3 . The difference in the percentage between the j th position and the best solution obtained is represented by $P_{(i,j)}$ with the help of Equation (7). In the current solution, the j th position is calculated.

$$P_{(i,j)} = \alpha + \frac{x_{(i,j)} - M(x_i)}{best_j(t) \times (UB_{(j)} - LB_{(j)}) + \epsilon} \quad (7)$$

$M(x_i)$, as defined in Equation (7), is the average position of the i th solution, as estimated by Equation (8). The upper and lower limits of the j th position are $UB_{(j)}$ and $LB_{(j)}$, respectively. The exploration precision (the difference among candidate solutions) for the hunting collaboration throughout the duration of iterations is controlled by alpha, which is set to 0.1 in this paper.

$$M(x_i) = \frac{1}{n} \sum_{j=1}^n x_{(i,j)} \quad (8)$$

3.4. Exploitation (Hunting Phase)

The exploitative behavior (hunting) of RSA is discussed in this section. Crocodiles use two hunting strategies: hunting cooperation and hunting coordination, according to their hunting behavior. These tactics refer to many intensive procedures that are dedicated to the exploitation hunt (local). Because crocodiles escalate, their escalation allows them to

approach the target prey readily, unlike encircling processes. As a result, the exploitation search finds the near-optimal solution, sometimes after numerous attempts. Furthermore, at this level of optimization, the exploitation techniques are used to perform an intensified search close to the optimal solution and to promote communication between them. The RSA exploitation methods use two major search strategies to exploit the search space and techniques to discover the best solution, which are (a) hunting cooperation, and (b) hunting coordination, which is shown in Equation (9). When $t \leq 3T/4$ and $t > 2T/4$ are present, the hunting coordination method is used; otherwise, when $t \leq T$ and $t > 3T/4$ are present, the hunting cooperation approach is used. To develop more dense solutions and utilize the promising zones (local), stochastic coefficients are evaluated. We used the simplest basic guideline, which may be used to replicate crocodile hunting behavior. The following locations updating Equation (9) are provided in this study for the exploitation phase:

$$x_{(i,j)}(t+1) = \begin{cases} best_j(t) \times P_{i,j} \times ran, & t \leq 3\frac{T}{4} \text{ and } t > 2\frac{T}{4} \\ best_j(t) - \eta_{(i,j)}(t) \times \epsilon - RP_{i,j} \times ran, & t \leq T \text{ and } t > 3\frac{T}{4} \end{cases} \quad (9)$$

Here, $best_j(t)$ denotes the j th position in the best solution obtained so far. The hunting function for the j th position in the i th solution is denoted by the letter $\eta_{(i,j)}$. The difference in the percentage between j th position and the best solution obtained is represented by $P_{(i,j)}$ with the help of Equation (7). The hunting function for the j th position in the i th solution is denoted by the letter $\eta_{(i,j)}$, which is obtained using Equation (4). ϵ is a very small value. The reduce function is indicated by $R_{(i,j)}$, which is a value that is calculated using Equation (5) to reduce the search area. Figures 2 and 3 indicate that when $t \leq T/2$, the encircling phase (exploration) is initiated, while when $t > T/2$, the hunting phase (exploitation) is initiated so that the attacker is near enough to the victim when attacking.

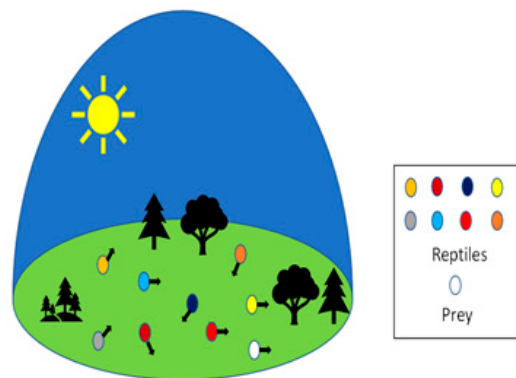


Figure 2. Encircling prey ($t \leq T/2$).

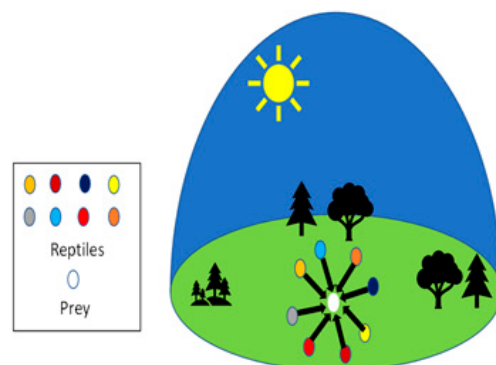


Figure 3. Attacking prey ($t > T/2$).

To avoid becoming caught in the local optima, exploitation search methods (hunting cooperation and hunting coordination) are used. These techniques aid the exploration search in selecting the best solution while also maintaining the diversity of candidate solutions. We carefully created two parameters (α and β) to generate a random number at every iteration, and we continued exploration not just during the first but also during the last iteration. This component of the search is useful when local optima stagnation occurs, especially in the last iteration.

3.5. Modeling

In RSA, the optimization handle starts with creating an arbitrary set of candidate solutions (population). RSA's look instrument analyzes the near-optimal positions of the near-redundant arrangement to detect redundancy. The positions of each arrangement are replaced by the best-obtained arrangement, which is in agreement with the RSA forms.

The search processes are divided into two categories (exploration and exploitation), with four strategies to emphasize exploitation and exploration. Exploitation: chasing coordination and corporation. Exploration: the belly walking strategy and high walking strategy candidate arrangement endeavor to expand the viewing region when $t \leq T/2$ and attempts to cover the near-optimal solution when $t > T/2$. In the stage of exploration, the walking movement is high, and this strategy is performed when $t \leq 2T/4$ and $t > T/4$. In the exploitation stage, the hunting coordinate strategy is performed when $t \leq 3T/4$ and $t \leq 2T/4$; otherwise, the hunting cooperation strategy is accomplished when $t \leq T$ and $t > 3T/4$. In the end, the RSA is stopped when it meets the final criterion. In Algorithm 1, the pseudocode for recommended RSA is described. The detailed process and intuitive RSA are shown in Figure 4.

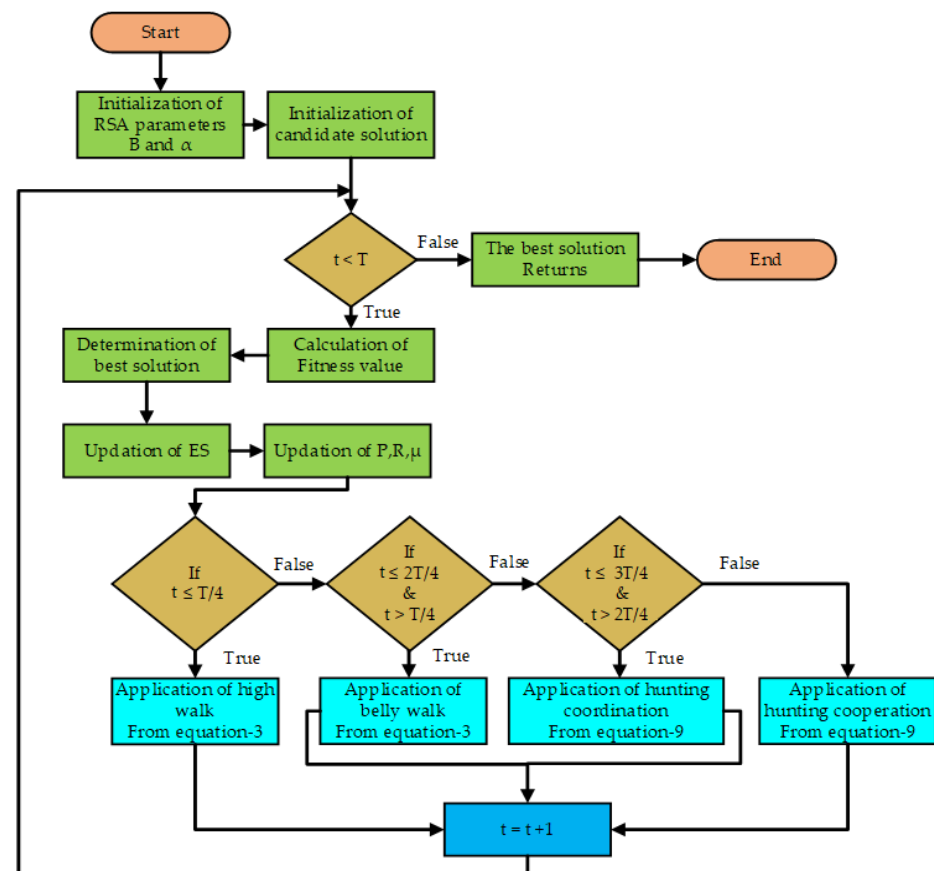


Figure 4. Flowchart of reptile search algorithm (RSA).

3.6. Time Complexity

The sophistication of the created RSA is determined by three primary parameters (i.e., initialization process, number of fitness evaluations, and solution updates), as shown below.

It is worth noting that the initialization procedure (N) has a computational complexity with solutions $O(N)$. The updating processes have a computational complexity of $O(T \times N) + (T \times N \times D)$. As a result, the proposed RSA's computational complexity is as follows.

Here, where T is the number of iterations, D denotes the size of the solution, and N denotes the number of solutions employed.

$$O(\text{RSA}) = O(N \times (T \times D + 1)) \quad (10)$$

4. Nine-Level Packed E-Cell (PEC-9)

4.1. PEC-9 Topology

The nine-level single-phase converter topology consists of six active bi-directional switches ($T1, T2, T3, T4, T5,$ and $T6$, constituting the PEC-9 topology), a DC voltage source (V_{dc}), a four-quadrant current device ($T7$), and two capacitors (C_a and C_b). The proposed topology is based on the concept of developing the auxiliary capacitor in a horizontal row layout using E-Cell type connections, as shown in Figure 5. Between the middle of the two capacitors and the inverter AC terminal point is a four-quadrant kind of switch. DC capacitors are arranged in a row in the E-Cell nine-level connection to generate a single auxiliary DC-link so that both capacitors can charge and discharge as desired [21–23]. As a result, during charging or discharging, both capacitors are synchronized, requiring balancing the auxiliary DC-link to intrinsically adjust the shunted capacitor's voltages to the necessary voltage level. Due to the four-quadrant switches, the E-Cell can create multi-output voltage levels, allowing for five, seven, or nine levels without changing the structure.

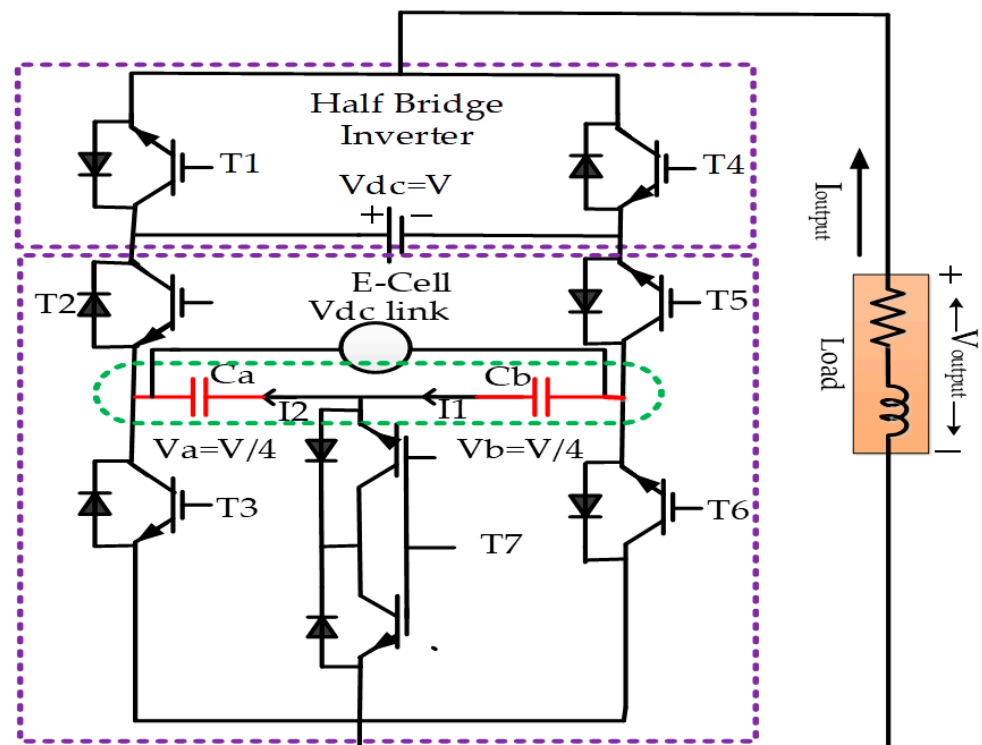


Figure 5. PEC-9 (nine-level Packed E-Cell) inverter topology.

4.2. Switching State Topology

Each of the Ca, Cb capacitors voltages (V_a , V_b) is balanced to one-quarter of the DC input voltage (V_{dc}) with the appropriate selection of switching states, resulting in PEC-9 generating a nine-level waveform. The switching states of the PEC-9 inverter are shown in Table 1. Switches (T1, T4), (T2, T5), and (T3, T6, T7) are complementary [24]. The charging and discharging mechanism of shunted capacitors, Ca and Cb, is determined by the load current direction. It is a charging state if the current is flowing into the capacitor from the positive side; otherwise, it is discharging state. Furthermore, when the capacitor is bypassed, the voltage does not change. Table 1 shows the voltages of capacitors in various states. As a result of the horizontal extension of the auxiliary DC-link, they have only one charging and discharging state in $\pm V/2$. Indeed, employing the E-Cell, one of the PEC advantages is that it may give the same discharging states and/or charging states for both capacitors.

Table 1. Switching states for PEC-9.

States	T1	T2	T3	T4	T5	T6	T7	I_{Output}	V_{Output}
1	1	0	0	0	1	1	0	+I	+V
2	1	0	0	0	1	0	1	+I	+3V/4
3	1	0	1	0	1	0	0	+I	+V/2
4	1	1	0	0	0	1	0	+I	+V/4
5	1	1	0	0	0	0	0	–	0
6	0	0	0	1	1	1	0	–I	–V/4
7	0	0	0	1	1	0	1	–I	–V/2
8	0	1	0	1	0	0	0	–I	–3V/4
9	0	1	1	1	0	0	0	–I	–V

The switching states of the levels 0 and $\pm V$ do not affect the output levels $\pm V/4$ and $\pm 3V/4$ when one capacitor is discharging or charging. It is to be noted that the low-frequency switches that are on the upper side (T1 and T2) are connected to the low-frequency DC source. At the switching frequency, other switches are operated. T1 and T2 (Upper switches) should tolerate the input DC voltage across the E-Cell's six remaining switches, an auxiliary DC-link voltage equal to half of the input DC. As a result, similarly, for the high-frequency component, switches at lower voltage can be used [25,26].

4.3. Fault-Tolerant Capability in PEC-9 Topology

As previously stated, E-Cell provides multiple-output AC terminal voltage, allowing for several voltage levels without changing the configuration, making PEC-9 a reliable topology. Let us assume that if a problem develops on a four-quadrant switch, PEC-9 will continue to operate. As the DC-link voltage is balanced to one-third or half of the DC input supply voltage, five or seven output voltage levels are possible [27]. Because the capacitors are linked in series, one capacitor C is assumed to be equivalent to half the value of C_a and C_b , while the four quadrant switch is in an open circuit condition during fault occurrences. For a five-level inverter, the DC-link voltage is controlled to half by redundant switching states or to one-third by a current controller to create seven voltage levels.

5. Implementation of the Reptile Search Algorithm in Selective Harmonic Elimination

In the method of pulse width modulation (PWM), the simple idea of the strategy is that the square output signal is chopped into multiple numbers. The chopping time is proportionate to a set of inverter's switching angles obtained by appropriate offline computations. The inverter bridge switch is turned ON and OFF with a suitable switching angle distribution. The output waveform of the inverter is adjusted to reduce lower-order harmonics. Invariant to carrier-based PWM techniques, instantaneous switching is determined by directly comparing the reference and carrier waveforms. The particular prominence of the switching versions is listed in the SHE method according to the

fundamental component desired and the harmonic component removed. The number of switching angles is generally kept to a minimum to maintain simple computations due to the complication of the equation that needs to be solved to locate switching instants. This is beneficial for minimizing instances of switching, and switching losses of the converter are calculated offline.

$$X(t) = V(t) = b_n \sin(n\omega t) \quad (11)$$

$$b_n = \frac{2}{2\pi} \int_0^{2\pi} f(\omega t) \times \sin(n\omega t) d\omega t \quad (12)$$

It is concluded by numerous studies that SHE pulse width modulation (SHE-PWM) is the best PWM approach. It efficiently reduces certain lower-order harmonics and eliminates the harmonic content from the inverter to provide the developed quality spectrum. This technique has been broadly used in electronic power controllers. The main idea is to place notches predominantly at selected PWM waveform places, and the inverter will sometimes modify the direction every half cycle to properly maintain the output waveform of the inverter. Since its inception, SHE pulse width modulation has sparked a lot of research curiosity. Specifically, it is being developed for high-power converters and high-voltage computers, where switching losses are a critical concern that must be reduced. SHE-PWM approaches decompose the PWM current/voltage waveform by applying Fourier analysis, and their performance is solely dictated by the formulation and characteristics of the waveform. Many waveform formulations have been analyzed and investigated in the technical literature, including unipolar, bipolar, and PWM multilevel and stepped waveforms. Likewise, wave characteristics such as symmetry, voltage levels, and amplitude play a fundamental role in analysis and solution establishment. SHE-PWM waveforms present an analytical challenge. Formulation of the waveform has a significant influence on the choice of an appropriate equation-solving algorithm. There are a variety of methods that can be used to obtain switching angles, such as iterative approaches, optimization techniques, and resultant theory, to solve various SHE-PWM waveforms. Multilevel converters have also been implemented for hybrid multilevels and a variety of other applications through SHE-PWM technology. Because a wide variety and a large number of multilevel converters are available, each topology needs a unique implementation to realize the potential benefits.

Switching Angle Calculation

A switch needs to have $(N - 1)/2$ switching angles to produce N levels of symmetrical quarter-wave output. Accordingly, the angles required are two, three, and four, respectively, for five, seven, and nine levels. Figure 6 shows an example of a nine-level output voltage. In addition, the SHE technique requires an additional firing angle to remove the next harmonic in every quarter cycle, $n + 1$. Consequently, a five-level output can eliminate only one (5th order) harmonic, a seven-level output can eliminate two (5th and 7th order), and a nine-level output can eliminate three (5th, 7th, and 9th order) harmonics.

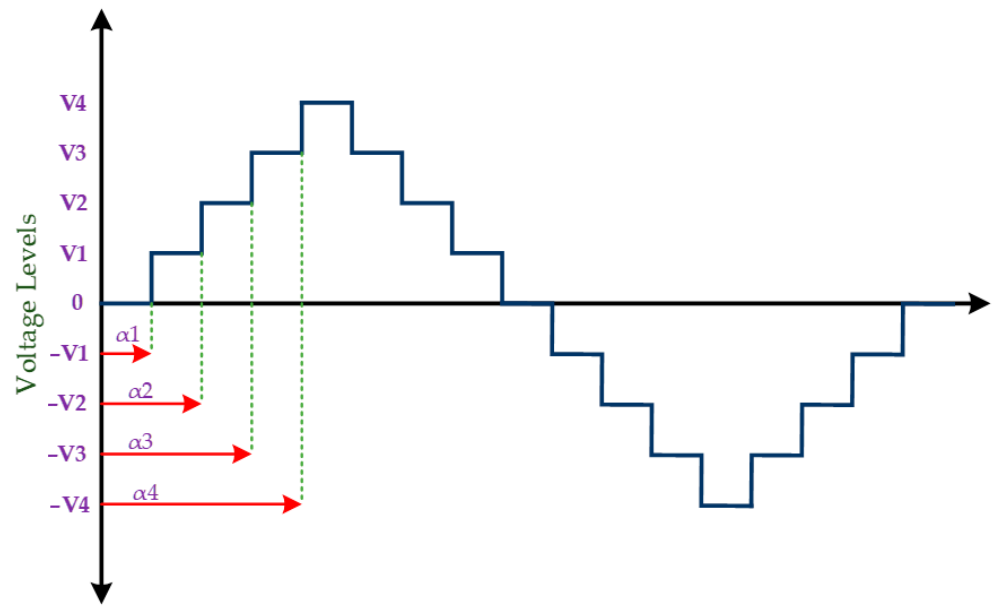


Figure 6. Nine-level output voltage.

Based on the Fourier series, we have an equation for each of the above nine levels. Because wave symmetry of the above nine levels is infrequent,

$$a_0 = 0 \text{ and } a_n = 0.$$

For the quarter-wave symmetry,

$$b_n = \left[\frac{2}{2\pi} \int_0^{\frac{\pi}{4}} f(\omega t) * \sin(n\omega t) d\omega t \right] \times 4 \quad (13)$$

$$\frac{4}{\pi} \left[\int_0^{\alpha_1} 0 \times \sin(n\omega t) d\omega t + \int_{\alpha_1}^{\alpha_2} (E_1 \times \sin(n\omega t) d\omega t) + \int_{\alpha_2}^{\alpha_3} (E_2 \times \sin(n\omega t) d\omega t) \right. \\ \left. + \int_{\alpha_3}^{\alpha_4} (E_3 \times \sin(n\omega t) d\omega t) + \int_{\alpha_4}^{\frac{\pi}{4}} (E_4 \times \sin(n\omega t) d\omega t) \right]$$

where

$$E_1 = V_{dc}, E_2 = 2V_{dc}, E_3 = 3V_{dc}, E_4 = 4V_{dc}.$$

$$b_n = \frac{4V_{dc}}{n\pi} [\cos(n\alpha_1) + \cos(n\alpha_2) + \cos(n\alpha_3) + \cos(n\alpha_4)] \quad (14)$$

$$V(t) = \sum_{n=1,3,5,\dots}^{\infty} \left(\frac{4V_{dc}}{n\pi} \times (\cos(n\alpha_1) + \cos(n\alpha_2) + \cos(n\alpha_3) + \cos(n\alpha_4)) \right) \sin(n\omega t)$$

For $n = \text{even}$.

$$b_n = 0$$

For $n = \text{odd}$.

$$b_n = \frac{4V_{dc}}{n\pi} [\cos(n\alpha_1) + \cos(n\alpha_2) + \cos(n\alpha_3) + \cos(n\alpha_4)]$$

Therefore, we have the Fourier series.

For K ($K = (N - 1)/2$) switching angles, we have:

$$V(t) = \sum_{n=1,3,5,\dots}^{\infty} \left(\frac{4V_{dc}}{n\pi} \times (\cos(n\alpha_1) + \cos(n\alpha_2) + \dots + \cos(n\alpha_k)) \right) \sin(n\omega t) \quad (15)$$

For nine levels, $K = 4$.

$$V_1 = \frac{4V_{dc}}{\pi} [\cos(\alpha_1) + \cos(\alpha_2) + \cos(\alpha_3) + \cos(\alpha_4)] \quad (16)$$

$$V_5 = \frac{4V_{dc}}{5\pi} [\cos(5\alpha_1) + \cos(5\alpha_2) + \cos(5\alpha_3) + \cos(5\alpha_4)] \quad (17)$$

$$V_7 = \frac{4V_{dc}}{7\pi} [\cos(7\alpha_1) + \cos(7\alpha_2) + \cos(7\alpha_3) + \cos(7\alpha_4)] \quad (18)$$

$$V_{11} = \frac{4V_{dc}}{11\pi} [\cos(11\alpha_1) + \cos(11\alpha_2) + \cos(11\alpha_3) + \cos(11\alpha_4)] \quad (19)$$

By equating V_1 , V_5 , V_7 , and V_{11} to zero, the required firing angle for eliminating the fifth, seventh, and eleventh harmonics may be calculated. Reptile search has been used in this paper to solve the above nonlinear equations. This gives the various values of α for different output voltage levels. It provides α_1 , α_2 , α_3 , and α_4 equal to 9.67° , 19.39° , 36.72° , and 55.83° for the output of nine levels at a 0.79 modulation index (m), and the computational parameters are given in Table 2.

Table 2. Computational parameters.

Parameters	Selection
No. of runs	25
No. of iterations	500
No. of crocodile (Space search)	30
No. of function evaluation	1500
α	0.1
β	0.1

6. Simulation Results

The output voltage of the PEC-9 model has been generated by MATLAB Simulink for nine levels. The midpoint of two capacitors and an inverter AC terminal point is connected between the four quadrant-type switches of the PEC-9 inverter topology, as shown in Figure 5, to implement a single auxiliary DC-link, and the DC capacitors are connected in a row so that the capacitor can be charged and discharged, respectively. Switching pulses were generated using IGBTs, and switching pulses were produced by repeating the sequence block. The parameters/components specifications used in MATLAB are shown in Table 3. A different set of firing angles has been calculated by RSA for several modulation indexes. Figure 7 illustrates the deviations of firing angles in nine levels (α_1 , α_2 , α_3 , and α_4) with different modulation indexes.

Table 3. MATLAB parameter simulation.

Sr. No.	Component/Parameter	Specification	Quantity/Component No.
1.	DC voltage source	600 V	1
2.	Power frequency	50 Hz	1
3.	IGBT	IKW40N65ES5	8
4.	load	50 Ω + 120 mH, 100 + 240 mH, 50 Ω , 100 Ω	R and RL type
5.	Capacitor	24,000 μ F	2

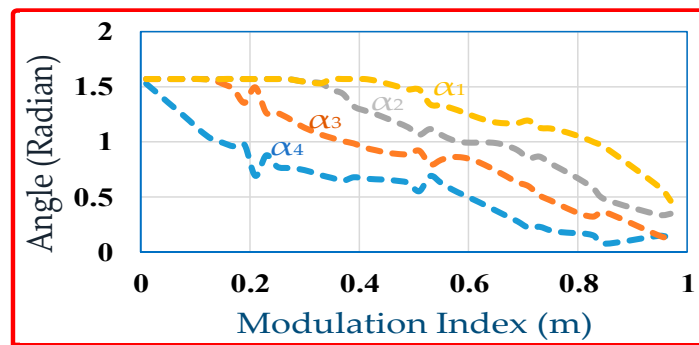


Figure 7. Firing angle (radian) versus modulation index (m) in PEC-9.

As shown in Figure 8, the outputs from the resistive load and the FFT profile were observed for nine levels. As illustrated in Figure 8, the 5th, 7th, and 9th harmonics have been removed from nine levels of output voltage. For both resistive and inductive loads, the effectiveness of the dynamic change in load has been simulated. In the beginning, the load was resistive, and its value changed dynamically from 50 to 100 Ω after 0.05 s. The profile of the current and voltage is illustrated in Figure 9, and the current waveform scale was multiplied by a factor of 15. Figure 10 shows the current and voltage waveform when a purely resistive load of 100 Ω changes dynamically to an inductive load of 100 Ω + 120 mH after 0.05 s. The output current and voltage waveforms for a dynamic inductive load change from 50 Ω + 120 mH to 100 Ω + 240 mH, as illustrated in Figure 11. The effect on the waveform of the current and voltage with a variation of DC voltage source from 600 to 300 V is shown in Figures 12 and 13, showing the output current and voltage waveform when the modulation index changes from 0.2 to 0.8 with a step of 0.2, and the current waveform scale is multiplied by a factor of one.

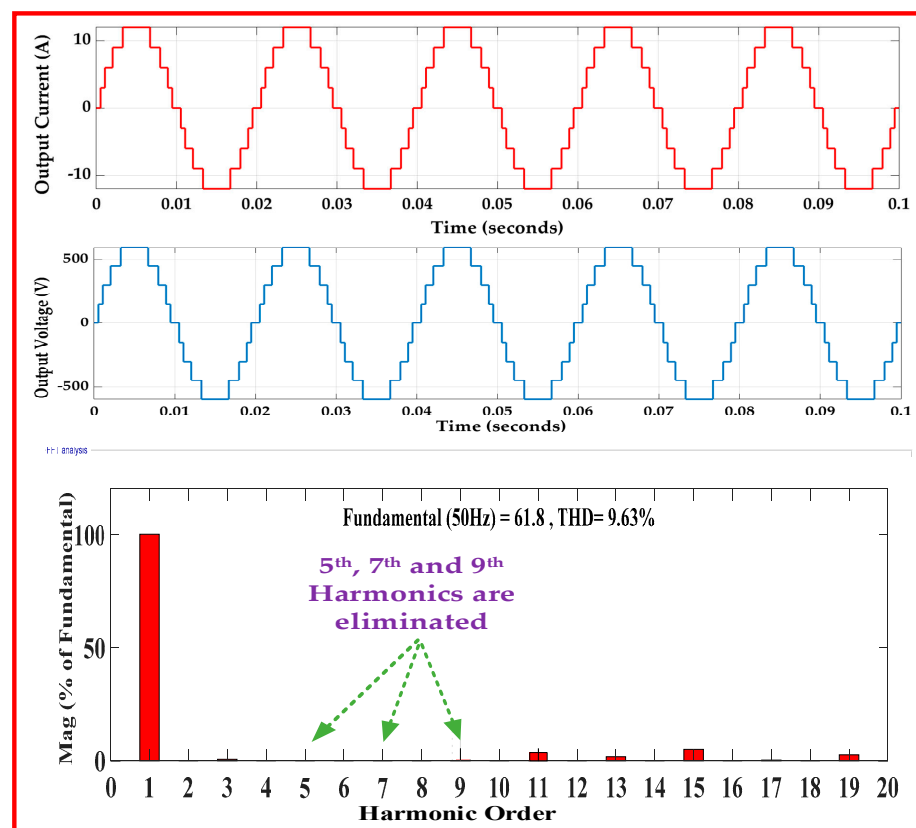


Figure 8. Harmonic profile and outputs of PEC-9.

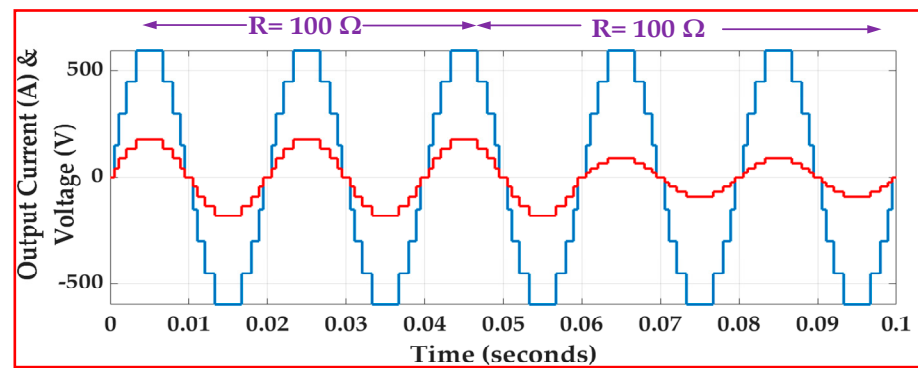


Figure 9. Dynamic resistive load change.

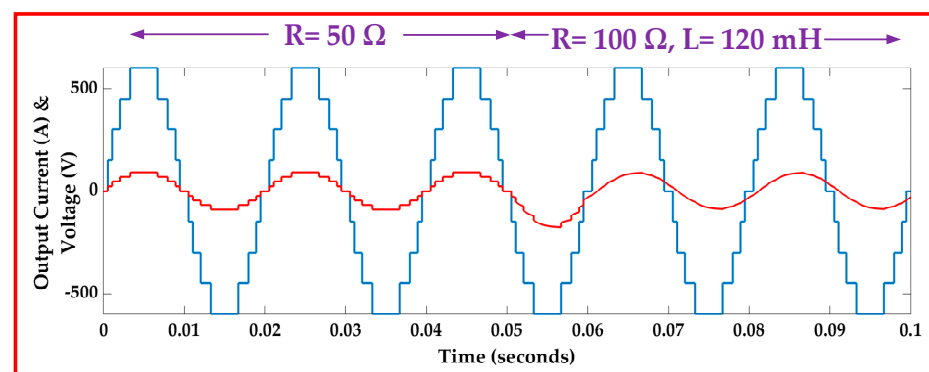


Figure 10. Dynamic resistive to inductive load change.

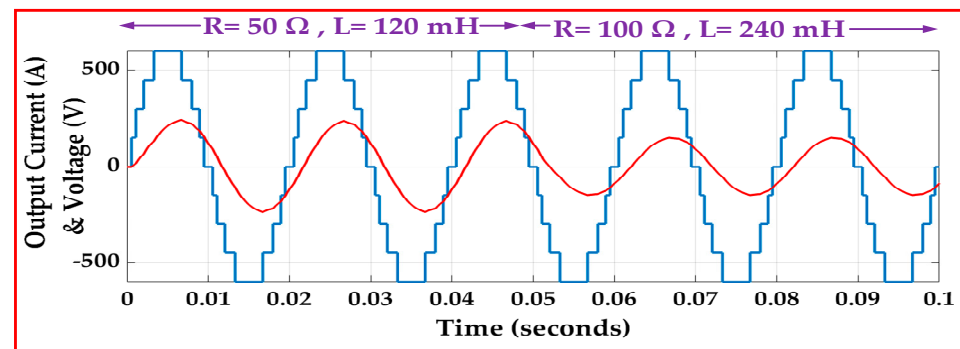


Figure 11. Dynamic inductive load change.

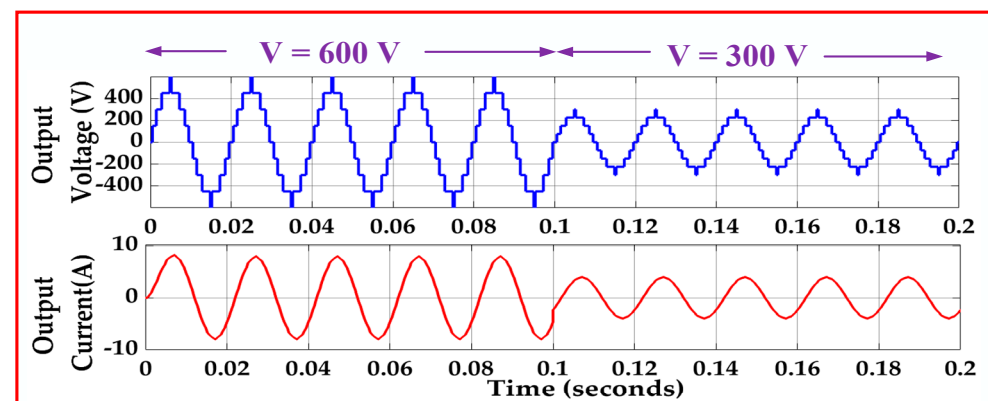


Figure 12. DC voltage source variation.

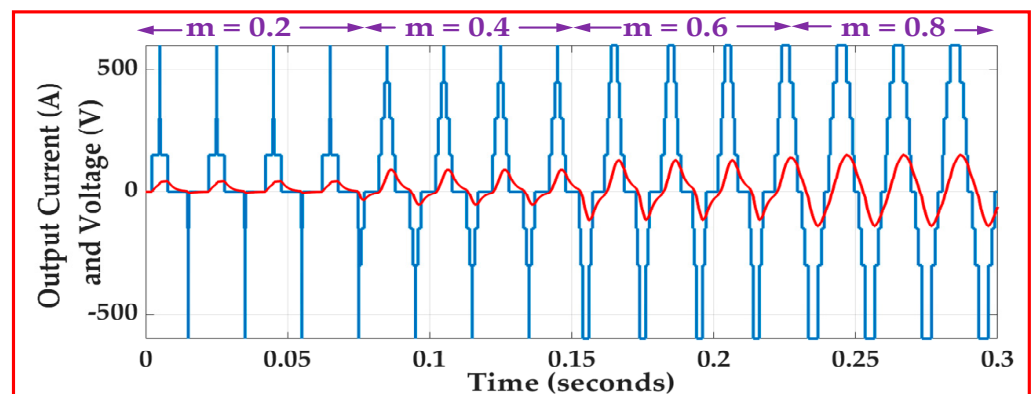


Figure 13. Modulation index (m) variation.

The THD for the nine-level inverter was compared using the genetic algorithm (GA), differential evolution (DE), and the reptile search algorithm (RSA), as shown in Figure 14. The graphs depict THD fluctuation as a function of the modulation index, which ranges from zero to one. THD is lower for RSA with an m of 0.35 in the case of the nine-level inverter. Between 0.4 and 0.6, DE has a superior result. From 0.6 to 0.65, GA performs best, whereas DE performs best from 0.64 to 0.7. The THD is almost the same for all techniques, with $m > 0.69$. Table 2 lists the parameter values used in the GA, DE, and RSA.

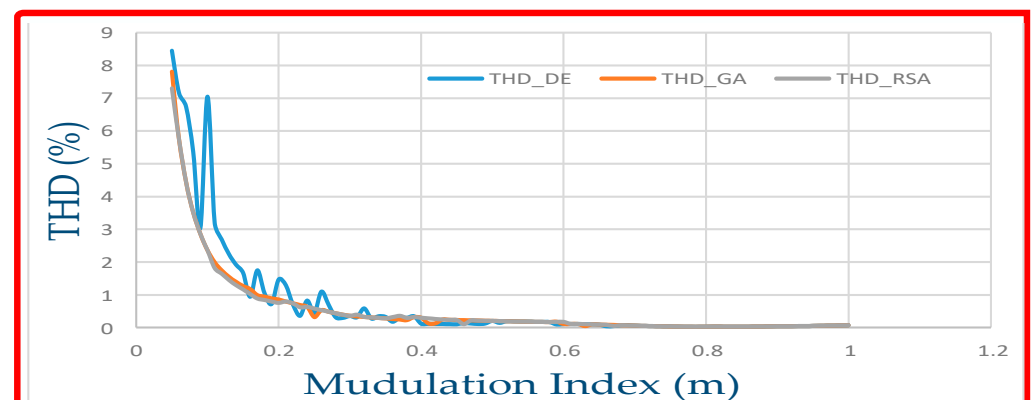


Figure 14. Different modulation index (m) variations of THD using RSA, DE, and GA for the nine-level inverter.

Although all of these approaches reduce the same selective harmonic, RSA improves THD in a broad range of modulation indexes. The statistical results show that the RSA can guarantee exploration effectiveness while delivering good exploitation, thereby preserving a balance between exploration and exploitation techniques, demonstrating the RSA's statistical superiority over other comparison algorithms.

7. Experimental Verification

On a Packed E-Cell (PEC-9) inverter prototype, the simulation results were experimentally validated in the laboratory. Eight (IKW40N65ES5) IGBTs are used in the prototype. TLP-250 is implemented as a gate driver circuit. To generate the control gate signal from the angles calculated by the RSA algorithm for IGBTs, a digital signal controller (TMS320F28335) was used. The firing angles were calculated by the RSA at a modulation index of 0.79 in three steps. To capture the current and voltage with respective harmonics, a TPS 2024 Tektronix oscilloscope was used. In Table 4, the specifications of the components used in the prototype are given. Figure 15 depicts the hardware arrangement used in the laboratory. Figure 16 shows the output current and voltage waveform for the RL load, and Figure 17 shows the output current and voltage waveform for the purely resistive load. Figure 18

illustrates the harmonic profile of the nine-level waveform. The waveform has a THD of 10.2 percent, which complies with optimal harmonic performance for a nine-level output. The 5th, 7th, and 9th harmonics were eliminated in the harmonic analysis result.

Table 4. Hardware parameters.

Sr. No.	Components	Specification
1.	IGBT	IKW40N65ES5
2.	Driver Circuit for IGBTs	TLP 250, 1 A
3.	DSP	TMS320F28335
4.	Input DC Source	200 V
5.	Load	$R = 30 \Omega$, $L = 30 \text{ mH}$
6.	Fundamental frequency	50 Hz

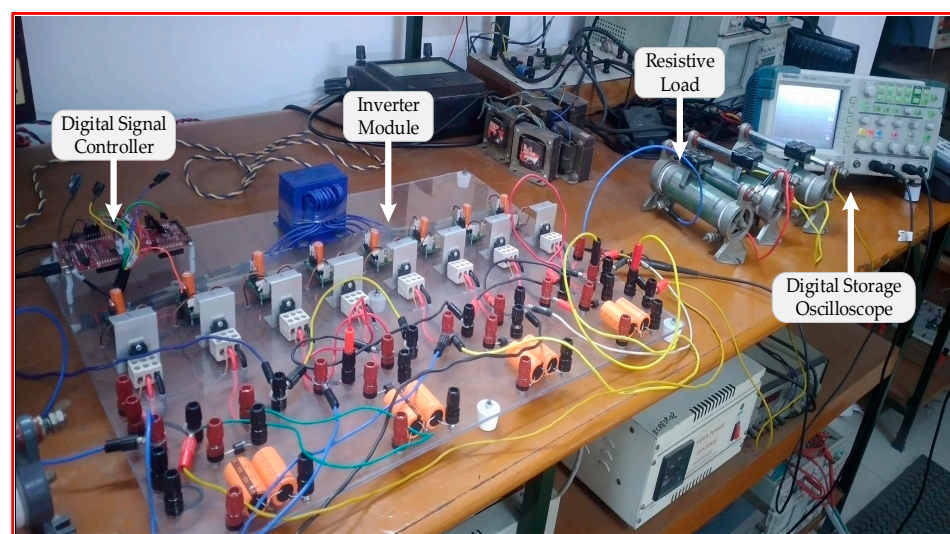


Figure 15. Laboratory experimental setup.

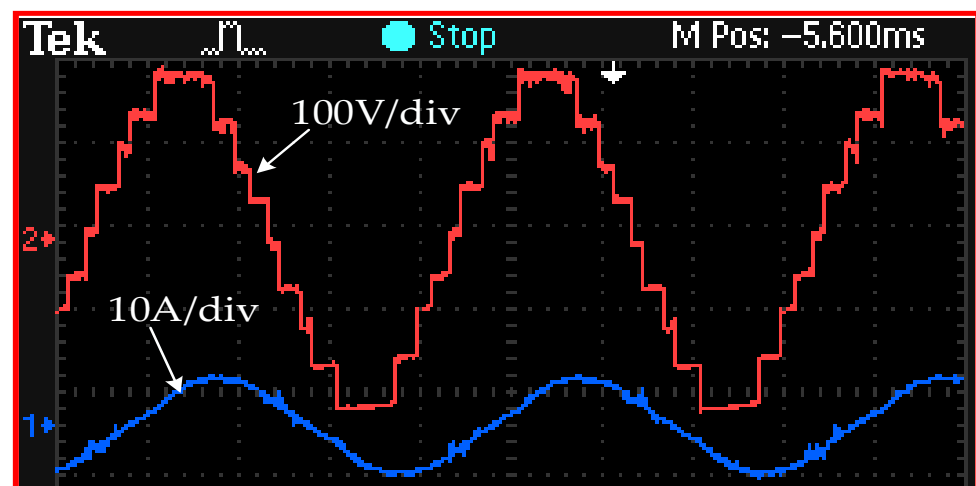


Figure 16. Voltage and current waveform at the RL load.

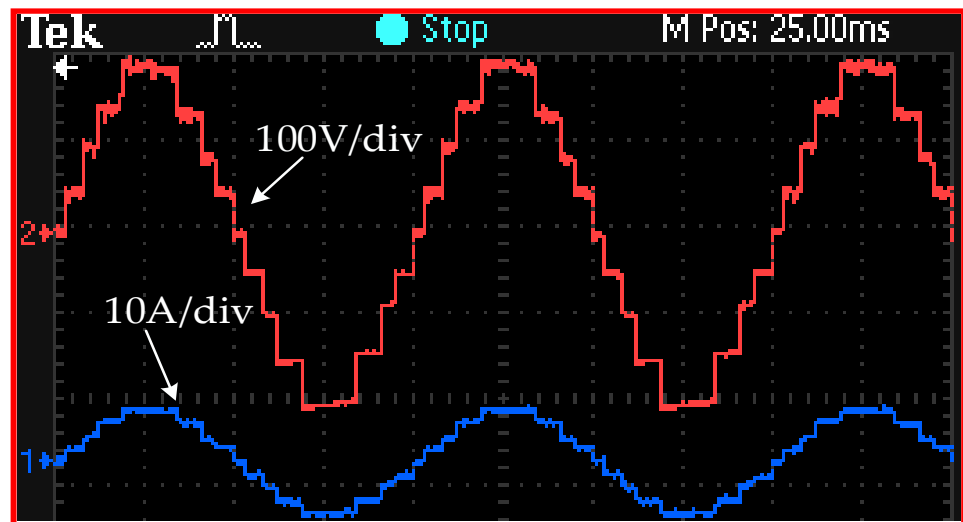


Figure 17. Voltage and current waveform at the R load.

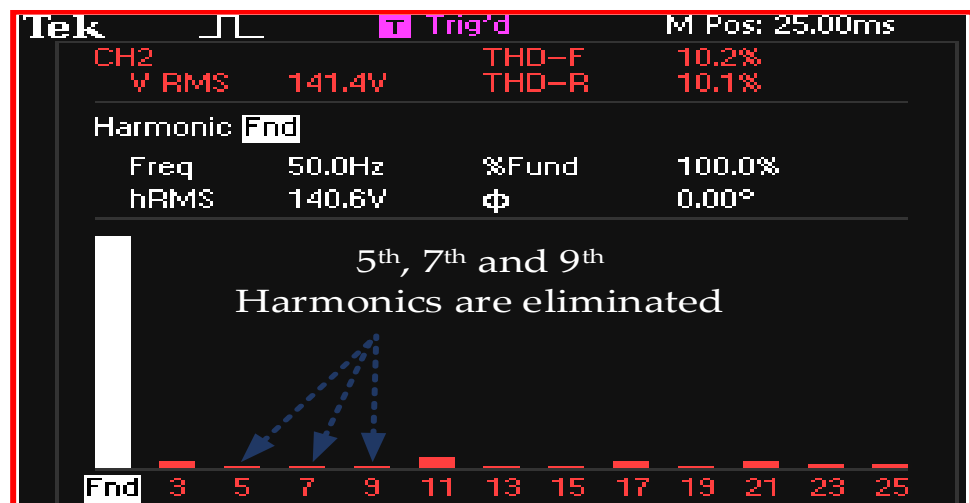


Figure 18. Harmonic profile.

8. Conclusions

By measuring the switching angle with the RSA and, therefore, eliminating the lower order harmonics, the THD of the output voltage of the PEC-9 has been improved. The SHE technique was used to remove low-order harmonics in nine-level inverters, and the results were analyzed. The RSA was used to solve nonlinear transcendental equations. The results reveal that the RSA outperforms various well-known metaheuristic algorithms such as DE and GA for a variety of modulation indexes. The elimination of these chosen harmonics resulted in a decrease in THD, which improved the inverter's performance. The experiment result, which is significantly closer to the simulation result, has been used to validate the total performance of PEC-9 with the optimal switching angle. The RSA is simple to implement, responds quickly, has a smooth curve of convergence, and only has a few control parameters. All of these things differentiate this algorithm from the others and also make it better to use. This method can be utilized in applications to solve a variety of real-life problems since it is flexible enough to produce optimized solutions to a variety of optimization problems. This method reduces the converter's THD and makes the converter more effective. As a result, this approach can be used to find the best possible solution to a given problem. For maximum output, this method can be used to build a maximum power point tracking (MPPT) system or to study a power system for optimal power distribution.

RSA has certain limitations, such as its inability to solve single-objective optimization problems with contested variables. Several research directions for future efforts can be recommended. Multiple discrete, multi-objective, and many-objective real-world optimization issues can be solved by extending the RSA's binary, modifications, and multi-objective variations.

Author Contributions: Conceptualization, R.A.K., B.S., A.S. and H.-D.L.; formal analysis, R.A.K. and B.S.; investigation, R.A.K. and C.-H.L.; software, R.A.K. and B.S.; methodology, R.A.K., B.S., A.S., C.-H.L. and H.-D.L.; data curation, R.A.K., B.S. and A.S.; visualization: R.A.K., B.S., A.S. and H.-D.L.; funding acquisition, A.S., C.-H.L. and H.-D.L.; supervision, A.S., H.-D.L. and C.-H.L.; writing—original draft, R.A.K. and B.S.; writing—review and editing, R.A.K., B.S., A.S. and H.-D.L. All authors have read and agreed to the published version of the manuscript.

Funding: This research was funded by the National Science and Technology Council, Taiwan, R.O.C., grant number MOST 111-2221-E-003-012. The authors also sincerely appreciate the considerable support from the National Taiwan Normal University Subsidy Policy to Enhance Academic Research Projects.

Institutional Review Board Statement: Not applicable.

Informed Consent Statement: Not applicable.

Data Availability Statement: Not applicable.

Acknowledgments: The authors also acknowledge the technical support provided by the Hardware-In-the-Loop (HIL) Lab and Non-Conventional Energy (NCE) Lab, Department of Electrical Engineering, Aligarh Muslim University, India. This research was funded by the National Science and Technology Council, Taiwan, R.O.C., grant number MOST 111-2221-E-003-012. The authors also sincerely appreciate the considerable support from the National Taiwan Normal University Subsidy Policy to Enhance Academic Research Projects.

Conflicts of Interest: The authors declare no conflict of interest.

References

1. Sharifzadeh, M.; Mehra, M.; Babaie, M.; Al-Haddad, K. Stable Frequency Response for Multi-Terminal MMC-HVDC System with DC Voltage Fluctuations. In Proceedings of the IECON 2019—45th Annual Conference of the IEEE Industrial Electronics Society, Lisbon, Portugal, 14–17 October 2019; pp. 3577–3582. [\[CrossRef\]](#)
2. Noghani, K.A.; Sharifzadeh, M.; Ounejjar, Y.; Al-Haddad, K. Current Based Model Predictive Control for DC Capacitor Optimization in Grid-Connected and Stand-Alone Nine-Level Packed U-Cell Inverter. In Proceedings of the 2019 IEEE 28th International Symposium on Industrial Electronics (ISIE), Vancouver, BC, Canada, 12–14 June 2019; pp. 787–792. [\[CrossRef\]](#)
3. Sajadi, R.; Iman-Eini, H.; Bakhshizadeh, M.K.; Neyshabouri, Y.; Farhangi, S. Selective harmonic elimination technique with control of capacitive DC-link voltages in an asymmetric cascaded H-bridge inverter for STATCOM application. *IEEE Trans. Ind. Electron.* **2018**, *65*, 8788–8796. [\[CrossRef\]](#)
4. el Gadari, A.; el Ouardi, H.; Alibou, S.; Ounejjar, Y.; Bejjit, L.; Sharifzadeh, M. New Nine-Level SPUC Inverter Using Single DC Source. In Proceedings of the IECON 2019—45th Annual Conference of the IEEE Industrial Electronics Society, Lisbon, Portugal, 14–17 October 2019; pp. 1892–1897. [\[CrossRef\]](#)
5. Sharifzadeh, M.; Babaie, M.; Sebaaly, F.; Mehra, M.; Chouinard, G.; Al-Haddad, K. Low Switching Frequency Operation of PEC9 Multilevel Inverter Using Modified SHM-PWM. In Proceedings of the IECON 2020 the 46th Annual Conference of the IEEE Industrial Electronics Society, Singapore, 18–21 October 2020; pp. 4215–4220. [\[CrossRef\]](#)
6. Sharifzadeh, M.; Vahedi, H.; Al-Haddad, K. SHM-PWM applied on single DC source CHB with self-regulation of capacitors voltages. In Proceedings of the 2018 IEEE International Conference on Industrial Technology (ICIT), Lyon, France, 20–22 February 2018; pp. 1893–1897. [\[CrossRef\]](#)
7. Khan, S.A. Performance Analysis of Nine-Level Packed E Cell Inverter for Different Carrier Wave PWM Techniques. In *AI and Machine Learning Paradigms for Health Monitoring System*; Springer: Singapore, 2021; pp. 419–427. [\[CrossRef\]](#)
8. Sharifzadeh, M.; Vahedi, H.; Al-Haddad, K. New Constraint in SHE-PWM for Single-Phase Inverter Applications. *IEEE Trans. Ind. Appl.* **2018**, *54*, 4554–4562. [\[CrossRef\]](#)
9. Jana, A.-S.; Liu, H.-D.; Lu, S.-D.; Lin, C.-H. New Control Scheme for Solar Power Systems under Varying Solar Radiation and Partial Shading Conditions. *Processes* **2021**, *9*, 1359. [\[CrossRef\]](#)
10. Siddique, M.D.; Mekhilef, S.; Padmanaban, S.; Memon, M.A.; Kumar, C. Single-Phase Step-Up Switched-Capacitor-Based Multilevel Inverter Topology with SHEPWM. *IEEE Trans. Ind. Appl.* **2021**, *57*, 3107–3119. [\[CrossRef\]](#)

11. Lu, S.-D.; Lin, C.-H.; Huang, L.-Y.; Lee, Y.-L.; Liu, H.-D.; Liao, P.-C.; Gao, G.-J.; Hsu, C.-M. Novel Global-MPPT Control Strategy Considering the Variation in the Photovoltaic Module Output Power and Loads for Solar Power Systems. *Processes* **2022**, *10*, 367. [[CrossRef](#)]
12. Liu, H.-D.; Lu, S.-D.; Lee, Y.-L.; Lin, C.-H. A Novel Photovoltaic Module Quick Regulate MPPT Algorithm for Uniform Irradiation and Partial Shading Conditions. *Processes* **2021**, *9*, 2213. [[CrossRef](#)]
13. Fahad, M. A Dual Source Switched-Capacitor Multilevel Inverter with Reduced Device Count. *Electronics* **2021**, *11*, 67. [[CrossRef](#)]
14. Islam, N.; Mohammad, K.; Khan, R.A.; Sarwer, Z.; Sarwar, A. Symmetrical and Asymmetrical Multilevel Inverter Topologies with Reduced Device Count: A Review. In Proceedings of the 2021 2nd International Conference for Emerging Technology (INCET), Belagavi, India, 21–23 May 2021; pp. 1–6. [[CrossRef](#)]
15. Sarwar, M.I.; Alam, M.S.; Ahmad, S.; Tariq, M. A Nine-Level Cascaded Multilevel Inverter with Reduced Switch Count and Lower Harmonics. In *Applications of Computing, Automation and Wireless Systems in Electrical Engineering*; Lecture Notes in Electrical Engineering; Springer: Singapore, 2019; p. 553. [[CrossRef](#)]
16. Sarwar, M.I.; Alam, M.S.; Sarwar, A.; M Zaid, A.R.; Sarfraz, M. PSO based Optimal Operation of a Cascaded Grid Connected Three Phase Solar PV Inverter. In Proceedings of the 2021 International Conference on Advances in Electrical, Computing, Communication and Sustainable Technologies (ICAECT), Bhilai, India, 19–20 February 2021; pp. 1–7. [[CrossRef](#)]
17. Fahad, M. Asymmetric Multilevel Inverter Topology and Its Fault Management Strategy for High-Reliability Applications. *Energies* **2021**, *14*, 4302. [[CrossRef](#)]
18. Khan, S.A.; Upadhyay, D.; Ali, M.; Rahman, K.; Tariq, M.; Sarwar, A.; Anees, A. Integration of Distributed PV System with Grid Using Nine-Level PEC Inverter. In *International Conference on Modelling, Simulation and Intelligent Computing*; Springer: Singapore, 2021; pp. 555–562. [[CrossRef](#)]
19. Khan, A.I. Artificial Neural Network-Based Maximum Power Point Tracking Method with the Improved Effectiveness of Standalone Photovoltaic System. In *AI and Machine Learning Paradigms for Health Monitoring System*; Springer: Singapore, 2021; pp. 459–470. [[CrossRef](#)]
20. Abualigah, L. Reptile Search Algorithm (RSA): A nature-inspired meta-heuristic optimizer. *Expert Syst. Appl.* **2022**, *191*, 116158. [[CrossRef](#)]
21. Farooqui, S.A. Crystal Structure Algorithm (CryStAl) Based Selective Harmonic Elimination Modulation in a Cascaded H-Bridge Multilevel Inverter. *Electronics* **2021**, *10*, 3070. [[CrossRef](#)]
22. Khan, R.A. Archimedes Optimization Algorithm Based Selective Harmonic Elimination in a Cascaded H-Bridge Multilevel Inverter. *Sustainability* **2021**, *14*, 310. [[CrossRef](#)]
23. Hussan, M.R. Aquila Optimization Based Harmonic Elimination in a Modified H-Bridge Inverter. *Sustainability* **2022**, *14*, 929. [[CrossRef](#)]
24. Khan, S.A. M-Type and CD-Type Carrier Based PWM Methods and Bat Algorithm-Based SHE and SHM for Compact Nine-Level Switched Capacitor Inverter. *IEEE Access* **2021**, *9*, 87731–87748. [[CrossRef](#)]
25. Farooqui, S.A.; Khan, R.A.; Islam, N.; Ahmed, N. Cuckoo Search Algorithm and Artificial Neural Network-based MPPT: A Comparative Analysis. In Proceedings of the 2021 IEEE 8th Uttar Pradesh Section International Conference on Electrical, Electronics and Computer Engineering (UPCON), Dehradun, India, 11–13 November 2021; pp. 1–5. [[CrossRef](#)]
26. Upadhyay, M.; Ali, M.; Tariq, M.; Khan, S.A.; Alamri, B.; Alahmadi, A. Thirteen-level UXE-type inverter with 12-band hysteresis current control employing PSO based PI controller. *IEEE Access* **2022**, *10*, 29890–29902. [[CrossRef](#)]
27. Sharifzadeh, M.; Al-Haddad, K. Packed E-Cell (PEC) Converter Topology Operation and Experimental Validation. *IEEE Access* **2019**, *7*, 93049–93061. [[CrossRef](#)]